Report

Current Biology

Anaeramoebae are a divergent lineage of eukaryotes that shed light on the transition from anaerobic mitochondria to hydrogenosomes

Highlights

- Deep transcriptomic sequencing of two new anaerobic metamonads
- The Anaeramoebae represents a new principal lineage of Metamonada
- Anaeramoebae are free-living relatives of the parasitic parabasalids
- Retention of mitochondrial features in mitochondrion-related organelles

Authors

Courtney W. Stairs, Petr Táborský, Eric D. Salomaki, ..., Jon Jerlström-Hultqvist, Andrew J. Roger, Ivan Čepička

Correspondence

courtney.stairs@biol.lu.se (C.W.S.), ivan.cepicka@centrum.cz (I.Č.)

In brief

Stairs et al. report a new phylum-level lineage of eukaryotes named the Anaeramoebae. These free-living anaerobes represent a new branch on the tree of life that is sister to the parasitic parabasalids, including *Trichomonas vaginalis*. The Anaeramoebae have complex mitochondrial proteomes with features not found in their closest relatives.

Stairs et al., 2021, Current Biology *31*, 5605–5612
December 20, 2021 © 2021 The Author(s). Published by Elsevier Inc.
https://doi.org/10.1016/j.cub.2021.10.010

CellPress

Current Biology

CellPress
OPEN ACCESS

Report

Anaeramoebae are a divergent lineage of eukaryotes that shed light on the transition from anaerobic mitochondria to hydrogenosomes

Courtney W. Stairs,[1,9,10,*] Petr Táborský,[2] Eric D. Salomaki,[3] Martin Kolisko,[3] Tomáš Pánek,[2] Laura Eme,[4] Miluše Hradilová,[5] Čestmír Vlček,[5] Jon Jerlström-Hultqvist,[6,7] Andrew J. Roger,[6,8] and Ivan Čepička[2,8,*]

[1]Department of Biology, Lund University, Sölvegatan 35, 223 62 Lund, Sweden
[2]Department of Zoology, Faculty of Science, Charles University, Viničná 7, 128 44 Prague, Czech Republic
[3]Institute of Parasitology, Biology Centre, Czech Academy of Sciences, 370 05 České Budějovice, Czech Republic
[4]Université Paris-Saclay, CNRS, AgroParisTech, Ecologie Systématique Evolution, 91400 Orsay, France
[5]Institute of Molecular Genetics, Academy of Sciences of the Czech Republic, Vídeňská 1083, 142 20 Prague, Czech Republic
[6]Department of Biochemistry and Molecular Biology, Dalhousie University, 5850 College St. Halifax, NS B3H 4R2, Canada
[7]Present address: Department of Cell and Molecular Biology, BMC, Box 596, Uppsala Universitet, 751 24 Uppsala, Sweden
[8]Senior author
[9]Twitter: @cstairs
[10]Lead contact
*Correspondence: courtney.stairs@biol.lu.se (C.W.S.), ivan.cepicka@centrum.cz (I.Č.)
https://doi.org/10.1016/j.cub.2021.10.010

SUMMARY

Discoveries of diverse microbial eukaryotes and their inclusion in comprehensive phylogenomic analyses have crucially re-shaped the eukaryotic tree of life in the 21st century.[1] At the deepest level, eukaryotic diversity comprises 9–10 "supergroups." One of these supergroups, the Metamonada, is particularly important to our understanding of the evolutionary dynamics of eukaryotic cells, including the remodeling of mitochondrial function. All metamonads thrive in low-oxygen environments and lack classical aerobic mitochondria, instead possessing mitochondrion-related organelles (MROs) with metabolisms that are adapted to low-oxygen conditions. These MROs lack an organellar genome, do not participate in the Krebs cycle and oxidative phosphorylation,[2] and often synthesize ATP by substrate-level phosphorylation coupled to hydrogen production.[3,4] The events that occurred during the transition from an oxygen-respiring mitochondrion to a functionally streamlined MRO early in metamonad evolution remain largely unknown. Here, we report transcriptomes of two recently described, enigmatic, anaerobic protists from the genus *Anaeramoeba*.[5] Using phylogenomic analysis, we show that these species represent a divergent, phylum-level lineage in the tree of metamonads, emerging as a sister group of the Parabasalia and reordering the deep branching order of the metamonad tree. Metabolic reconstructions of the *Anaeramoeba* MROs reveal many "classical" mitochondrial features previously not seen in metamonads, including a disulfide relay import system, propionate production, and amino acid metabolism. Our findings suggest that the cenancestor of Metamonada likely had MROs with more classical mitochondrial features than previously anticipated and demonstrate how discoveries of novel lineages of high taxonomic rank continue to transform our understanding of early eukaryote evolution.

RESULTS

Anaeramoebae reorder the phylogeny of Metamonada

To deepen our understanding of the phylogenetic placement and metabolic potential of the Anaeramoebae, we sequenced the transcriptomes of *Anaeramoeba ignava* and *Anaeramoeba flamelloides*[5] (Figures 1A and 1B). Using these data, we performed a phylogenomic analysis with representatives from all major eukaryote lineages (Figures 1C and S1). We found that the two *Anaeramoeba* species form a clade that branches as sister to the Parabasalia within a monophyletic Metamonada; all three relevant branches receive full support in maximum likelihood (ML) bootstrap analyses (Figures 1D and S1) and in Bayesian analysis (FigShare: https://doi.org/10.6084/m9.figshare.12205517.v1).

Metamonada is represented by three major lineages (phyla)—Preaxostyla (e.g., *Trimastix*, *Monocercomonoides*), Fornicata (e.g., *Carpediemonas*, *Giardia*), and Parabasalia (e.g., *Trichomonas*, *Tritrichomonas*).[6] To date, nearly all phylogenetic investigations recover Parabasalia and Fornicata as sister lineages to the exclusion of Preaxostyla, including a recent analysis that placed *Barthelona*, a genus of free-living flagellates, as sister to the Fornicata with 100% bootstrap support.[7] Support for the relationship between Fornicata and Parabasalia has not wavered,

This is an open access article under the CC BY license (http://creativecommons.org/licenses/by/4.0/).

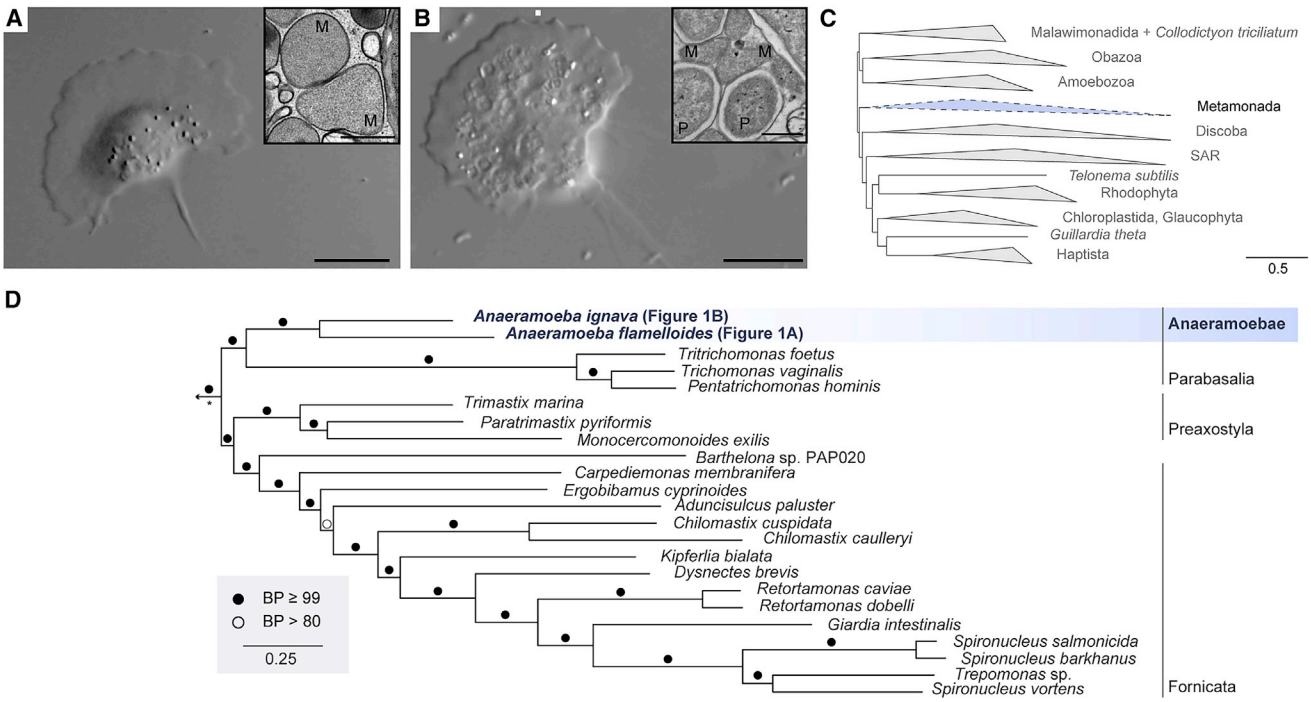

Figure 1. Anaeramoebae are the closest free-living relatives of parabasalids

Differential interference contrast micrographs of living amoebae of *Anaeramoeba flamelloides* (A) and *A. ignava* (B). Insets: Transmission electron micrographs of the cells of *Anaeramoeba* species showing MROs (M) and prokaryotic symbionts (P); scale bar: 10 μm; inset scale bar: 0.5 μm. (C and D) Phylogenomic analysis is inferred from 95 taxa, 155 proteins, and 53,637 sites. Bipartition support values derived from 1,000 non-parametric bootstraps (LG+C60+F+G+PMSF model of evolution) are mapped onto the ML tree estimated with IQTREE under the LG+C60+F+G model of evolution. Support values greater than or equal to 99 or greater than 80 are shown in closed and open circles, respectively. All bipartitions were recovered with posterior probability = 1.0 in Bayesian analyses with CAT+GTR, except the monophyly of Metamonada indicated with *. Tree files for all analyses are available at FigShare: https://doi.org/10.6084/m9.figshare.12205517.v1 (see Figure S1 for uncollapsed tree).

despite the potential for long branch attraction (LBA) between these lineages, as Fornicata and Parabasalia contain some of the longest branches in eukaryote phylogenies.[3,8–10] In the analyses presented here, adding the *Anaeramoeba* species, which are among the shortest branches of any known metamonad, breaks the long stem branch leading to the parabasalids and supports the monophyly of Preaxostyla, *Barthelona*, and Fornicata to the exclusion of the *Anaeramoeba*+Parabasalia clade.

We tested whether alternative hypotheses could be rejected by the data using approximately unbiased (AU) topology tests. The topology constraining the monophyly of Parabasalia+Fornicata+*Barthelona* was rejected ($p = 0.00311$; Data S1), suggesting that this previously reported relationship is unlikely to be correct. Topologies constraining the monophyly of Parabasalia+Fornicata+*Anaeramoeba*+*Barthelona* ($p = 0.0263$), Discoba+Metamonada+*Collodictyon*+*Malawimonas* ($p = 0.00263$), and the Phylobayes consensus topology (*Malawimonas*+Fornicata+*Barthelona*+Preaxostyla; $p = 3.66 \times 10^{-5}$) were all rejected.

We hypothesize that the clade composed of Preaxostyla, *Barthelona*, and Fornicata, recovered herein, is the result of improved taxon sampling and the use of a sophisticated substitution model for phylogenetic inference (i.e., the LG+C60+F+G model; Figure 1) that together have offset an LBA artifact previously grouping Parabasalia with *Barthelona* and Fornicata, to the exclusion of Preaxostyla. Thus, the inclusion of Anaeramoebae in analyses fundamentally changes the deep structure of the Metamonada tree.[3,8–10]

Anaeramoebids and parabasalids have dissimilar morphologies

The close relationship between Parabasalia and Anaeramoebae is surprising because members of these two groups are quite dissimilar on a morphological and ultrastructural level.[5] Anaeramoebids are predominantly amoeboid organisms with cell structures and motility reminiscent of certain members of the supergroup Amoebozoa.[5] They contain an acentriolar centrosome, from which sparse, individual microtubules radiate. In contrast, most parabasalids are flagellates with intricate cytoskeletons composed of large microtubular and non-microtubular networks. Although several parabasalids (e.g., *Dientamoeba fragilis* and *Trichomonas vaginalis*) have amoeboid characteristics, these species form terminal branches in the phylogenetic tree of Parabasalia; their ability to move using pseudopodia appears to have arisen independently from that of anaeramoebids.[11] Two out of six known *Anaeramoeba* species, including *A. ignava*, have been shown to have a flagellate stage[5] with a unique morphology, distinct from that of other flagellated protists including Parabasalia.[5] Moreover, Parabasalia possess a conspicuously stacked Golgi apparatus, known as the parabasal body,[11] yet we could not identify a "stacked" Golgi in anaeramoebids when using several microscopical techniques.[5] Since

CellPress
OPEN ACCESS

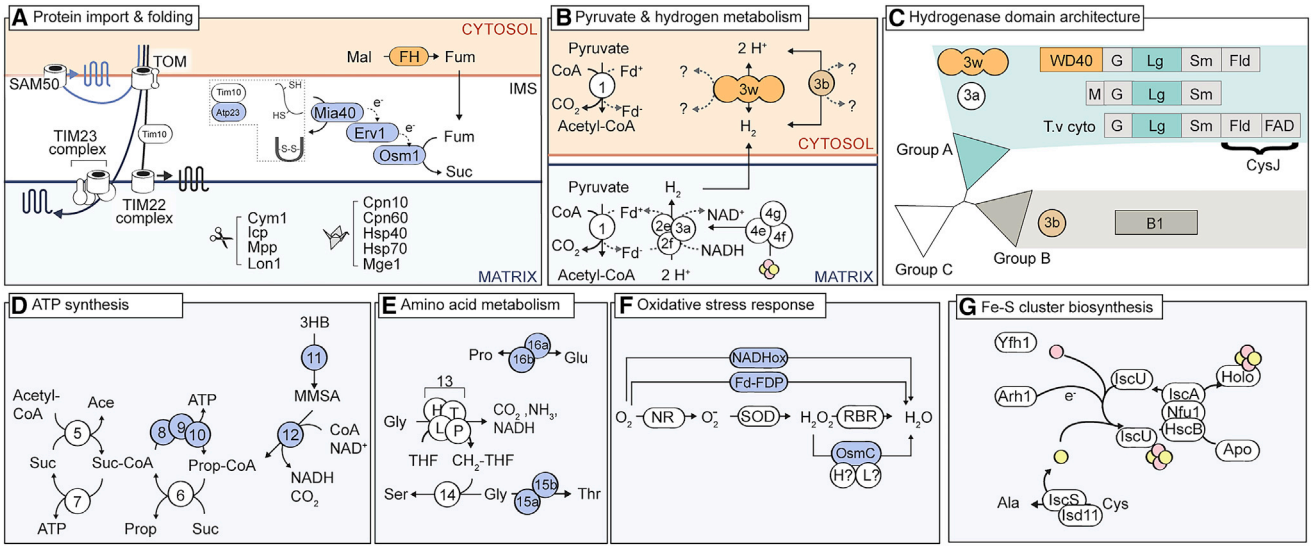

Figure 2. Selected metabolic pathways related to protein import and folding, pyruvate and hydrogen metabolism, energy metabolism, amino acid metabolism, oxidative stress response, and Fe-S cluster biosynthesis

Proteins that have previously not been identified in metamonads are shown in blue and orange, representing putative MRO or cytoplasmic localization, respectively. Protein domain architectures of hydrogenase proteins are shown: "WD40", WD-40 domain; "G", NADH dehydrogenase subunit G (IPR019574); "Lg", large hydrogenase subunit (IPR004108); "Sm", small hydrogenase subunit (IPR004108); "Fld", flavodoxin domain (IPR001094); "FAD", FAD-binding domain (IPR017927). Detailed list of chaperones (crane) and proteases (scissors) can be found in Data S1. Abbreviations: 1,PFO; 2, NADH:ubiquinone oxidoreductase E and F; 3, [FeFe]-hydrogenase: Group A (3a), WD40-GroupA (3w) and Group B (3b); 4, [FeFe]-hydrogenase E-G; 5, ASCT type 1C; 6, ASCT 1B; 7, SCS; 8, Methylmalonyl (MM)-CoA epimerase; 9, MM-CoA mutase; 10, Propionyl-CoA (Prop-CoA) carboxylase; 11, 3HB dehydrogenase; 12, MM-semialdehyde (MMSA) dehydrogenase; 13, glycine (gly) cleavage system H,P,L,T proteins; 14, serine (ser) hydroxymethyltransferase; 15, Threonine (Thr) biosynthesis: Thr dehydrogenase (a) and Thr synthase (b); 16, D-pyrroline-5-carboxylate (DPC) dehydrogenase (a) and pyrroline-5-carboxylate reductase (b); NADHox, NADH oxidase; Fd-FDP, Ferredoxin-flavodiiron protein; NR, nitrate reductase; SOD, superoxide dismutase; RBR, rubrerythrin; OsmC, peroxidase; Yfh1, Frataxin; IscS, Isd11, Cysteine desulphurase; IscU, IscA Fe-S scaffold proteins; Arh1, ferredoxin reductase; Ace, acetate; Suc, succinate; Prop, propionate; Pro, proline; Glu, glutamate; Fd, ferredoxin; SAM, sorting and assembly machinery; IMS, intermembrane space. See also Figure S2 and Data S1.

the anaeramoebids are fundamentally distinct from the three main metamonad phyla,[6] we propose that they belong in a new phylum, Anaeramoebae.[5]

Anaeramoebid MROs have the most complete protein import machinery among metamonads

Previous microscopic examinations indicated that anaeramoebids possess mitochondrion-related organelles (MROs)[5] (Figures 1A and 1B). We therefore sought to reconstruct the mitochondrial proteome from the transcriptomic data. We identified 102 and 122 proteins that are predicted to function in the MROs of *A. ignava* and *A. flamelloides*, respectively, based on homology to known mitochondrial or MRO proteins and/or predicted mitochondrial localization (Data S1). We found no evidence of transcripts encoding proteins related to mitochondrial genome (mtDNA) maintenance or expression, suggesting that, like all other metamonad MROs, anaeramoebid MROs lack mtDNA. Below, we discuss the pathways that have not been observed in metamonads before (Figure 2, blue and orange shaded circles).

Most mitochondrion- or MRO-targeted proteins are transcribed from nuclear genes, translated in the cytoplasm, and imported into mitochondrial compartments by the translocase of the outer mitochondrial membrane (TOM) and translocase of the inner mitochondrial membrane (TIM) following recognition of N-terminal or internal targeting signals. We observed that anaeramoebids have a similar complement of TOM and TIM components previously described in *Trichomonas vaginalis*[12] (Figures 2A and 3). However, we identified components of the intermembrane space (IMS) and its disulfide relay system that have never been identified in any metamonad. This system is necessary for the import and folding of some proteins destined for the IMS.[13] Mia40 is an IMS-localized oxidoreductase that, together with the sulfhydryl oxidase Erv1, generates disulfide bonds into its substrate proteins.[13,14] Under aerobic conditions, yeast Mia40-Erv1 transfers electrons from substrate proteins to oxygen or cytochrome *c*. However, under anaerobic conditions, electrons can be transferred to fumarate via the IMS-localized fumarate reductase Osm1.[15,16] We identified homologs of the relay system (Mia40, Erv1, and Osm1), a cytoplasmic class II fumarate hydratase (FH), and two putative Mia40 substrates: the IMS protease Atp23 and Tim10 (Figure 2A). In yeast, Atp23 processes the Atp6 subunit of ATP synthase[17] and controls the protein turnover of other IMS proteins linked to lipid metabolism such as Ups1.[18] Using the *Anaeramoeba* proteins as queries, we were able to detect Atp23-like proteins in the parabasalids *Trichomonas vaginalis* and *Tritrichomonas foetus* (Data S1). Given that parabasalids and anaeramoebids do not encode any components of ATP synthase or Ups1, Atp23 likely has another substrate. Future phylogenomic profiling or cell biological investigations should consider querying the reduced MRO proteomes of parabasalids and anaeramoebids to identify other Atp23 substrates that are conserved across eukaryotes.

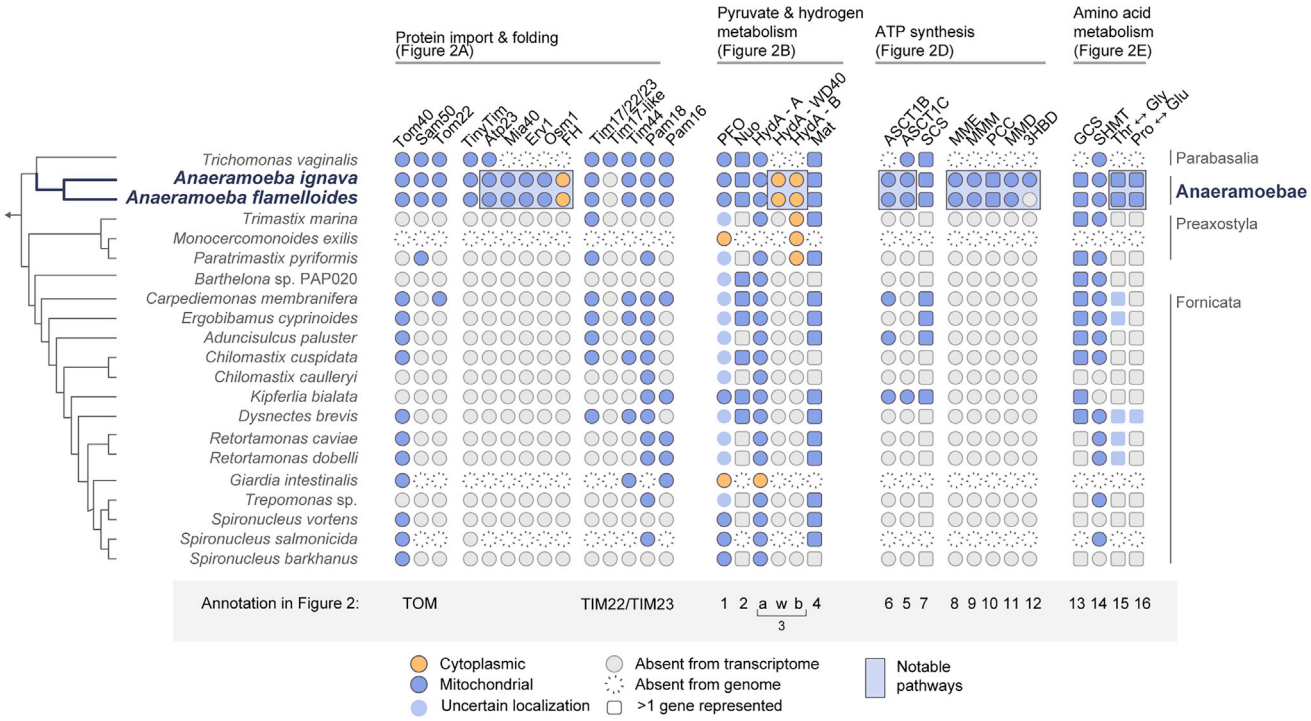

Figure 3. Distribution of various MRO functions across Metamonada

Publicly available genome and transcriptome projects were surveyed for genes encoding various MRO proteins. Those proteins predicted to function in the cytoplasm or MRO are shown in orange and blue, respectively. For hydrogen metabolism, some organisms have multiple HYDA genes with protein products predicted to localize in the cytoplasm or MRO; therefore, blue circles indicate that at least one protein is predicted to function in the MRO. "WD40" denotes whether a HYDA protein with an N-terminal WD40 domains was identified. If a gene encoding the protein was not found in a transcriptome or genome, it is denoted with a hashed or gray icon, respectively. For visualization purposes, pathways or enzymes with more than one protein are shown with squares. Abbreviations and numbers are as shown in Figure 2. See Data S1 for sequence data for all metamonad proteins indicated. We failed to detect the *Trichomonas*-specific TIM17-like subunit,[19] suggesting that this protein likely evolved specifically along the parabasalid lineage. See also Figures S2 and S3 and Data S1.

The targeting of proteins to the mitochondrial matrix is often dependent on the recognition of a positively charged N-terminal targeting signal (NTS). Many *Anaeramoeba* MRO matrix proteins with complete N-termini (*A. ignava*: 35/72 [48.6%] and *A. flamelloides* 51/86 [59.3%]) have NTSs with a net positive charge (Data S1). This is in contrast to observations in *Trichomonas*, where only 10% (39/359) of experimentally localized hydrogenosomal proteins have detectable NTSs, and they do not have a net positive charge.[20] Similar observations have been made in *Giardia*.[12] In *Trichomonas*, this suggests that the majority of hydrogenosomal proteins are imported via cryptic targeting signals.[20] This loss of NTS-dependent import in *Trichomonas* hydrogenosomes could derive from the loss of the respiratory-chain-driven membrane potential that is critical for the import of positively charged NTSs.[20] Our observation of positively charged NTS-dependent protein import in *Anaeramoeba* MROs—organelles that are not predicted to have a respiratory-chain-driven membrane potential—has an number of implications: (1) the positively charged NTS-dependent import of proteins can exist in MROs that do not have a respiratory chain, such as *Anaeramoeba* species; (2) *Anaeramoeba* MROs might have a membrane potential that is generated independent of a respiratory chain;[21] and/or (3) the loss of positively charged NTS-dependent import likely occurred twice independently along the Parabasalia and Fornicata lineages. Future experimental investigations of the MRO proteomes of *Anaeramoeba* species are needed to confirm that positively charged NTSs are major features of their MRO targeting systems.

Anaeramoebids encode hydrogenosomal and cytoplasmic hydrogen metabolism

The hydrogenosomes of *Trichomonas* oxidize pyruvate via pyruvate:ferredoxin oxidoreductase (PFO) to generate acetyl-CoA, CO_2, and reduced ferredoxin (Fd^-). Electrons from Fd^- and NADH are used by a trimeric, electron-confurcating [FeFe]-hydrogenase (HYDA, NUOE, and NUOF). The proper assembly of the HYDA subunit requires three MRO-localized maturase proteins (HYDE-G). We identified homologs of PFO, HYDA, NUOE, NUOF, and the maturase proteins in both *A. ignava* and *A. flamelloides* that are predicted to function in the MRO (Figure 2B; Data S1). We detected two types of HYDA corresponding to the Group A and Group B hydrogenases[22] (Figures 2C and S2; STAR Methods). We identified numerous copies of Group A hydrogenases in both anaeramoebid species, predicted to function in the MRO or cytoplasm; however, the Group B hydrogenases are predicted to be exclusively cytoplasmic.

Some of the putatively cytoplasmic anaeramoebid Group A HYDA proteins have N-terminal extensions that encode WD40 domains that have not been previously reported to be fused to HYDA proteins (Figures 3 and S2). WD40 domains are abundant

in most eukaryotic proteomes and are often considered interaction hubs for protein-protein interaction networks.[23] Since WD40-domain-containing proteins often interact with other WD40-domain-containing proteins,[23] we manually investigated every predicted protein that contains a WD40 domain (IPR020472) to identify potential interaction partners. We failed to detect any WD40-domain-containing proteins that contain an additional domain related to electron transfer reactions.

Without biochemical characterization, we cannot be confident about the direction of the reactions catalyzed by the putative HYDA enzymes. We suspect that "canonical" MRO-localized Group A HYDA functions as part of a trimeric, electron-confurcating, H_2-evolving hydrogenase as proposed in *Trichomonas*.[24,25] The function of the remaining Group A HYDA proteins or the Group B HYDA proteins in eukaryotes has not been explored *in vitro*. It has been suggested that the cytoplasmic Group A HYDA proteins of *Trichomonas* might function in the consumption of H_2 under certain conditions.[26] Therefore, the anaeramoebid cytoplasmic Group A or Group B HYDA proteins may oxidize H_2 produced by the MRO. If so, intracellular H_2-cycling could be ancestral to the Parabasalia+Anaeramoebae group or even the entire Metamonada lineage.

NADH- and Fd-coupled electron confurcation that is catalyzed by the multimeric hydrogenases (e.g., NUOE-NUOF-HYDA) is only thermodynamically favorable at low partial pressures of hydrogen.[27] Therefore, H_2-evolving bacteria and eukaryotes often grow syntrophically with other organisms who consume H_2[28–30]. Intracellular H_2-cycling has even been documented within a single bacterial cell.[31] In syntrophic eukaryotic systems, the H_2-evolving organelle is often spatially associated with the H_2-consumer.[28–30] We observed a similar spatial organization between the MROs and proposed prokaryotic symbionts of both *Anaeramoeba* species in transmission electron micrographs.[5] This suggests that the symbionts and MROs might exchange metabolites (e.g., H_2).

Anaeramoebid MROs have more ATP-producing pathways than *Trichomonas vaginalis* hydrogenosomes

In *Trichomonas vaginalis*, the acetyl-CoA generated from the PFO reaction is converted to acetate via acetate:succinate CoA transferase (ASCT subtype 1C) to generate succinyl-CoA, which can serve as a substrate for the Krebs cycle enzyme succinyl-CoA synthetase (SCS), ultimately synthesizing ATP.[32] We detected proteins related to hydrogenosomal-type ATP production in both *Anaeramoeba* species (Figure 2D). Unlike all other metamonads studied to date, the anaeramoebids also encode the methylmalonyl-CoA pathway for the synthesis of ATP. In aerobic mitochondria and the mitochondrial compartment of some anaerobes,[33] succinyl-CoA is converted to propionyl-CoA with the concomitant production of ATP by the actions of methylmalonyl-CoA epimerase, methylmalonyl-CoA mutase, and propionyl-CoA carboxylase. The CoA moiety of propionyl-CoA is transferred to succinate by ASCT 1B to generate propionate and succinyl-CoA, respectively. We also detected homologs of 3-hydroxybutyrate (3HB) dehydrogenase for the conversion of 3HB to methylmalonylate semialdehyde. This represents the first evidence for propionate synthesis in Metamonada. We hypothesize that the propionate and acetate produced by the MRO could be key metabolites supporting the syntrophic interaction between *Anaeramoeba* and its symbionts as seen in other eukaryote:prokaryote syntrophies.[30]

Anaeramoebid MROs have versatile amino acid interconversion pathways

Mitochondria are responsible for the biosynthesis and interconversion of some amino acids.[34] A common feature retained in MROs in free-living protists[3,35] is the mitochondrial glycine cleavage system (GCS; Figure 2E) necessary for the generation of methylene tetrahydrofolate (CH_2-THF) from glycine for serine biosynthesis. We identified a putatively MRO-localized GCS and serine hydroxymethyltransferase in both anaeramoebid species. We also detected proteins involved in proline and glutamate interconversion and threonine synthesis (Figure 2E) that are only sparsely distributed across other metamonads (Figure 3), suggesting that anaeramoebid MROs retain the most ancestral, mitochondrion-like repertoire of amino acid biosynthesis capabilities among metamonads.

Other pathways

Oxygen and reactive oxygen species can oxidize DNA, lipids, and proteins; therefore, most eukaryotes have strategies to prevent and repair oxidative damage in all compartments of the cell, including mitochondria/MROs. In the hydrogenosomes of *Trichomonas vaginalis*, oxygen is metabolized directly to water via flavodiiron protein (FDP), NADH oxidase (NADHox), or the concerted action of nitrate reductase (NR), superoxide dismutase (SOD), and rubrerythrin (RBR) (Figure 2F).

We identified homologs of NADHox, NR, SOD, and RBR in the *Anaeramoeba* species, (Figure 2F) along with two FDPs predicted to function in the cytoplasm (FDP-Rb) and MRO (Fd-FDP) with distinct evolutionary histories and domain organization (see Figure S3A). We noted that the MRO-targeted FDP (Fd-FDP) had an N-terminal 2Fe-2S Fd domain (IPR036010) in addition to the core FDP domains (IPR036866 and IPR029039) (Figure S3A). The *T. vaginalis* homolog of this enzyme (Genbank: XP_001583562.1), which lacks a Fd domain, uses electrons derived from pyruvate or NADH via the Fd electron carrier for oxygen detoxification.[36] Therefore, it is possible that the Anaeramoebid Fd-FDP fusion proteins interact directly with NADH- (NUOE, NUOF) or pyruvate- (PFO) producing enzymes to reduce oxygen.

To detoxify hydrogen peroxide, *Trichomonas vaginalis* hydrogenosomes can use the peroxidase OsmC/Ohr together with the H- and L-protein components of the GCS[37] (Figure 2F). We identified OsmC/Ohr-like proteins in *A. ignava*, one of which was predicted to function in the MRO (Data S1). We also identified OsmC/Ohr homologs in the transcriptomes of other metamonads; however, these sequences were too fragmented to predict their subcellular localization. In phylogenetic analyses, the metamonad OsmC/Ohr proteins formed a paraphyletic group, suggesting these proteins might have distinct evolutionary histories (Figure S3B). Whether the *A. ignava* OsmC/Ohr-like protein functions with the GCS proteins cannot be determined at present. If the *Anaeramoeba* and *Trichomonas* proteins do have distinct evolutionary origins, it suggests that this oxygen stress response pathway has convergently evolved in two related lineages.

Nearly all mitochondria and related organelles studied to date function in the biosynthesis of Fe-S clusters. In most organelles,

these cofactors are synthesized by the iron-sulfur cluster (ISC) system. We identified all the major components of the ISC system in both species of *Anaeramoeba* (Figure 2G; Data S1). We also found numerous mitochondrial carrier family proteins (SLC25A) that are predicted to transport nucleotides, S-adenosylmethionine, folate, iron, and carnitine (Data S1).

DISCUSSION

The Anaeramoebae are an anciently diverged metamonad lineage that represent the long-sought-after, free-living sister group of the predominantly parasitic Parabasalia. The inclusion of Anaeramoebae in phylogenomic analyses leads to a crucial rearrangement of the higher-order metamonad relationships; the two fundamental groups within Metamonada appear to be an Anaeramoebae+Parabasalia clade and a Fornicata+*Barthelona*+Preaxyostyla group. The discovery and robust phylogenetic placement of the Anaeramoebae within the tree of metamonads has important implications to future investigations on the adaptation to host and anaerobic environments that occurred in the evolution of the parabasalid lineage. For example, genomes of Anaeramoebae could be surveyed for proteins homologous to those involved in host-pathogen interactions in parabasalids to investigate how and when molecular systems for pathogenesis originated in this lineage.

Our analyses predict that the Anaeramoebae possess hydrogen-producing MROs that have the most "mitochondrion-like" proteome of all metamonads and utilize positively charged NTSs for protein import. These MROs represent important "missing links" between typical aerobic mitochondria of other eukaryote supergroups and anaerobic MROs of the Metamonada. Collectively, these findings allow us to hypothesize that the last common ancestor of Metamonada was a phagocytosing heterotroph that resided in low-oxygen environments, engaged in syntrophic interactions with prokaryotes (through metabolite exchange), and possessed MROs with more canonical mitochondrial features than previously anticipated.

STAR★METHODS

Detailed methods are provided in the online version of this paper and include the following:

- KEY RESOURCE TABLE
- RESOURCE AVAILABILITY
  - Lead contact
  - Materials availability
  - Data and code availability
- EXPERIMENTAL MODEL AND SUBJECT DETAILS
  - Culturing conditions for *Anaeramoeba ignava* and *Anaeramoeba flamelloides*
- METHOD DETAILS
  - RNA isolation and sequencing
  - Read decontamination, transcriptome assembly, and annotation
  - Phylogenomic dataset assembly
  - Phylogenomic tree reconstruction
- QUANTIFICATION AND STATISTICAL ANALYSIS
  - Investigation of select relationships in the phylogenomic analyses
  - Investigation of select relationships in phylogenetic analyses of genes related to hydrogen metaoblism and the oxygen stress response

SUPPLEMENTAL INFORMATION

Supplemental information can be found online at FigShare: https://doi.org/10.1016/j.cub.2021.10.010.

ACKNOWLEDGMENTS

I.C., P.T., and T.P. were supported by the Czech Science Foundation (project 18-18699S). C.W.S. is supported by the Swedish Research Council (Vetenskapsrådet starting grant 2020-05071). Work carried out in the Roger lab was supported by foundation grant FRN-142349, awarded to A.J.R. by the Canadian Institutes of Health Research. L.E. is supported by funding from the European Research Council (ERC StG 803151). E.D.S. was supported by the MSCA-IF SMART (CZ.02.2.69/0.0/0.0/20_079/0017809). M.K. was supported by Czech Science Foundation (project 18-28103S). This project was also supported by ERD fund "Centre for Research of Pathogenicity and Virulence of Parasites" (no. CZ.02.1.01/0.0/0.0/16_019/0000759). T.P. has been supported by Charles University Research Centre program no. 204069. The authors would like to thank Diogo Meireles for supplying OsmC/Ohr protein family alignments.[38] The authors would like to thank the IT4Innovations National Super Computer Center, Technical University of Ostrava, Ostrava, Czech Republic for access to the HPC resources (projects Open-21-29). This article is dedicated to the memory of Prof. Thomas Cavalier-Smith, a scientist and educator who inspired protistologists worldwide.

AUTHOR CONTRIBUTIONS

Conceptualization, C.W.S., T.P., P.T., M.K., A.J.R., and I.C.; methodology, C.W.S., E.D.S., L.E., M.K., T.P., and P.T.; software, C.W.S., E.D.S., L.E., M.K., T.P., and P.T.; formal analysis, C.W.S., E.D.S., L.E., M.K., T.P., P.T., A.J.R., and I.C.; investigation, C.W.S., E.D.S., L.E., M.K., P.T., J.J,-H., M.H., and C.V.; resources, T.P., J.J.-H., A.J.R., and I.C.; data curation, C.W.S., T.P., E.D.S., L.E., M.K., P.T., A.J.R., and I.C.; writing – original draft, C.W.S., L.E., M.K., T.P., A.J.R., and I.C.; writing – review & editing, C.W.S., E.D.S., L.E., M.K., T.P., A.J.R., and I.C.; visualization, C.W.S. and E.D.S.; supervision, C.W.S., M.K., A.J.R., and I.C.; project administration, C.W.S., M.K., A.J.R., and I.C.; funding acquisition, A.J.R. and I.C.

DECLARATION OF INTERESTS

The authors declare no competing interests.

Received: March 4, 2021
Revised: July 7, 2021
Accepted: October 5, 2021
Published: October 27, 2021

REFERENCES

1. Burki, F., Roger, A.J., Brown, M.W., and Simpson, A.G.B. (2020). The New Tree of Eukaryotes. Trends Ecol. Evol. *35*, 43–55.
2. Stairs, C.W., Leger, M.M., and Roger, A.J. (2015). Diversity and origins of anaerobic metabolism in mitochondria and related organelles. Philos. Trans. R. Soc. Lond. B Biol. Sci. *370*, 20140326.
3. Leger, M.M., Kolisko, M., Kamikawa, R., Stairs, C.W., Kume, K., Čepička, I., Silberman, J.D., Andersson, J.O., Xu, F., Yabuki, A., et al. (2017). Organelles that illuminate the origins of *Trichomonas* hydrogenosomes and *Giardia* mitosomes. Nat. Ecol. Evol. *1*, 0092.
4. Jerlström-Hultqvist, J., Einarsson, E., Xu, F., Hjort, K., Ek, B., Steinhauf, D., Hultenby, K., Bergquist, J., Andersson, J.O., and Svärd, S.G. (2013).

Hydrogenosomes in the diplomonad Spironucleus salmonicida. Nat. Commun. *4*, 2493.

5. Táborský, P., Pánek, T., and Čepička, I. (2017). Anaeramoebidae fam. nov., a Novel Lineage of Anaerobic Amoebae and Amoeboflagellates of Uncertain Phylogenetic Position. Protist *168*, 495–526.
6. Adl, S.M., Bass, D., Lane, C.E., Lukeš, J., Schoch, C.L., Smirnov, A., Agatha, S., Berney, C., Brown, M.W., Burki, F., et al. (2019). Revisions to the Classification, Nomenclature, and Diversity of Eukaryotes. J. Eukaryot. Microbiol. *66*, 4–119.
7. Yazaki, E., Kume, K., Shiratori, T., Eglit, Y., Tanifuji, G., Harada, R., Simpson, A.G.B., Ishida, K.-I., Hashimoto, T., and Inagaki, Y. (2020). Barthelonids represent a deep-branching metamonad clade with mitochondrion-related organelles predicted to generate no ATP. Proc. Biol. Sci. *287*, 20201538.
8. Takishita, K., Kolisko, M., Komatsuzaki, H., Yabuki, A., Inagaki, Y., Čepička, I., Smejkalová, P., Silberman, J.D., Hashimoto, T., Roger, A.J., and Simpson, A.G. (2012). Multigene phylogenies of diverse Carpediemonas-like organisms identify the closest relatives of 'amitochondriate' diplomonads and retortamonads. Protist *163*, 344–355.
9. Heiss, A.A., Kolisko, M., Ekelund, F., Brown, M.W., Roger, A.J., and Simpson, A.G.B. (2018). Combined morphological and phylogenomic re-examination of malawimonads, a critical taxon for inferring the evolutionary history of eukaryotes. R. Soc. Open Sci. *5*, 171707.
10. Hampl, V., Hug, L., Leigh, J.W., Dacks, J.B., Lang, B.F., Simpson, A.G.B., and Roger, A.J. (2009). Phylogenomic analyses support the monophyly of Excavata and resolve relationships among eukaryotic "supergroups". Proc. Natl. Acad. Sci. USA *106*, 3859–3864.
11. Čepička, I., Dolan, M.F., and Gile, G.H. (2016). Parabasalia. In Handbook of the Protists, , J.M. Archibald, A.G.B. Simpson, C.H. Slamovits, L. Margulis, M. Melkonian, D.J. Chapman, and J.O. Corliss, eds. (Springer International Publishing), pp. 1–44.
12. Doležal, P., Makki, A., and Dyall, S.D. (2019). Protein Import into Hydrogenosomes and Mitosomes. In Hydrogenosomes and Mitosomes: Mitochondria of Anaerobic Eukaryotes Microbiology Monographs, , J. Tachezy, ed. (Springer International Publishing), pp. 31–84.
13. Backes, S., and Herrmann, J.M. (2017). Protein Translocation into the Intermembrane Space and Matrix of Mitochondria: Mechanisms and Driving Forces. Front. Mol. Biosci. *4*, 83.
14. Reinhardt, C., Arena, G., Nedara, K., Edwards, R., Brenner, C., Tokatlidis, K., and Modjtahedi, N. (2020). AIF meets the CHCHD4/Mia40-dependent mitochondrial import pathway. Biochim Biophys Acta Mol Basis Dis *1866*, 165746.
15. Neal, S.E., Dabir, D.V., Wijaya, J., Boon, C., and Koehler, C.M. (2017). Osm1 facilitates the transfer of electrons from Erv1 to fumarate in the redox-regulated import pathway in the mitochondrial intermembrane space. Mol. Biol. Cell *28*, 2773–2785.
16. Williams, C.C., Jan, C.H., and Weissman, J.S. (2014). Targeting and plasticity of mitochondrial proteins revealed by proximity-specific ribosome profiling. Science *346*, 748–751.
17. Osman, C., Wilmes, C., Tatsuta, T., and Langer, T. (2007). Prohibitins interact genetically with Atp23, a novel processing peptidase and chaperone for the F_1F_o-ATP synthase. Mol. Biol. Cell *18*, 627–635.
18. Potting, C., Wilmes, C., Engmann, T., Osman, C., and Langer, T. (2010). Regulation of mitochondrial phospholipids by Ups1/PRELI-like proteins depends on proteolysis and Mdm35. EMBO J. *29*, 2888–2898.
19. Rada, P., Doležal, P., Jedelský, P.L., Bursac, D., Perry, A.J., Šedinová, M., Smíšková, K., Novotný, M., Beltrán, N.C., Hrdý, I., et al. (2011). The core components of organelle biogenesis and membrane transport in the hydrogenosomes of Trichomonas vaginalis. PLoS ONE *6*, e24428.
20. Garg, S., Stölting, J., Zimorski, V., Rada, P., Tachezy, J., Martin, W.F., and Gould, S.B. (2015). Conservation of Transit Peptide-Independent Protein Import into the Mitochondrial and Hydrogenosomal Matrix. Genome Biol. Evol. *7*, 2716–2726.
21. Stairs, C.W., Eme, L., Brown, M.W., Mutsaers, C., Susko, E., Dellaire, G., Soanes, D.M., van der Giezen, M., and Roger, A.J. (2014). A SUF Fe-S cluster biogenesis system in the mitochondrion-related organelles of the anaerobic protist Pygsuia. Curr. Biol. *24*, 1176–1186.
22. Greening, C., Biswas, A., Carere, C.R., Jackson, C.J., Taylor, M.C., Stott, M.B., Cook, G.M., and Morales, S.E. (2016). Genomic and metagenomic surveys of hydrogenase distribution indicate H2 is a widely utilised energy source for microbial growth and survival. ISME J. *10*, 761–777.
23. Stirnimann, C.U., Petsalaki, E., Russell, R.B., and Müller, C.W. (2010). WD40 proteins propel cellular networks. Trends Biochem. Sci. *35*, 565–574.
24. Müller, M., Mentel, M., van Hellemond, J.J., Henze, K., Woehle, C., Gould, S.B., Yu, R.-Y., van der Giezen, M., Tielens, A.G.M., and Martin, W.F. (2012). Biochemistry and evolution of anaerobic energy metabolism in eukaryotes. Microbiol. Mol. Biol. Rev. *76*, 444–495.
25. Hrdý, I., Hirt, R.P., Doležal, P., Bardonová, L., Foster, P.G., Tachezy, J., and Embley, T.M. (2004). Trichomonas hydrogenosomes contain the NADH dehydrogenase module of mitochondrial complex I. Nature *432*, 618–622.
26. Sutak, R., Hrdý, I., Doležal, P., Cabala, R., Sedinová, M., Lewin, J., Harant, K., Müller, M., and Tachezy, J. (2012). Secondary alcohol dehydrogenase catalyzes the reduction of exogenous acetone to 2-propanol in Trichomonas vaginalis. FEBS J. *279*, 2768–2780.
27. Stams, A.J.M., and Plugge, C.M. (2009). Electron transfer in syntrophic communities of anaerobic bacteria and archaea. Nat. Rev. Microbiol. *7*, 568–577.
28. Beinart, R.A., Beaudoin, D.J., Bernhard, J.M., and Edgcomb, V.P. (2018). Insights into the metabolic functioning of a multipartner ciliate symbiosis from oxygen-depleted sediments. Mol. Ecol. *27*, 1794–1807.
29. Finlay, B.J., Esteban, G., Clarke, K.J., Williams, A.G., Embley, T.M., and Hirt, R.P. (1994). Some rumen ciliates have endosymbiotic methanogens. FEMS Microbiol. Lett. *117*, 157–161.
30. Hamann, E., Gruber-Vodicka, H., Kleiner, M., Tegetmeyer, H.E., Riedel, D., Littmann, S., Chen, J., Milucka, J., Viehweger, B., Becker, K.W., et al. (2016). Environmental Breviatea harbour mutualistic Arcobacter epibionts. Nature *534*, 254–258.
31. Wiechmann, A., Ciurus, S., Oswald, F., Seiler, V.N., and Müller, V. (2020). It does not always take two to tango: "Syntrophy" via hydrogen cycling in one bacterial cell. ISME J. *14*, 1561–1570.
32. van Grinsven, K.W.A., Rosnowsky, S., van Weelden, S.W.H., Pütz, S., van der Giezen, M., Martin, W., van Hellemond, J.J., Tielens, A.G.M., and Henze, K. (2008). Acetate:succinate CoA-transferase in the hydrogenosomes of Trichomonas vaginalis: identification and characterization. J. Biol. Chem. *283*, 1411–1418.
33. Pietrzak, S.M., and Saz, H.J. (1981). Succinate decarboxylation to propionate and the associated phosphorylation in Fasciola hepatica and Spirometra mansonoides. Mol. Biochem. Parasitol. *3*, 61–70.
34. Spinelli, J.B., and Haigis, M.C. (2018). The multifaceted contributions of mitochondria to cellular metabolism. Nat. Cell Biol. *20*, 745–754.
35. Zubáčová, Z., Novák, L., Bublíková, J., Vacek, V., Fousek, J., Rídl, J., Tachezy, J., Doležal, P., Vlček, C., and Hampl, V. (2013). The mitochondrion-like organelle of Trimastix pyriformis contains the complete glycine cleavage system. PLoS ONE *8*, e55417.
36. Smutná, T., Gonçalves, V.L., Saraiva, L.M., Tachezy, J., Teixeira, M., and Hrdý, I. (2009). Flavodiiron protein from *Trichomonas vaginalis* hydrogenosomes: the terminal oxygen reductase. Eukaryot. Cell *8*, 47–55.
37. Nývltová, E., Smutná, T., Tachezy, J., and Hrdý, I. (2016). OsmC and incomplete glycine decarboxylase complex mediate reductive detoxification of peroxides in hydrogenosomes of Trichomonas vaginalis. Mol. Biochem. Parasitol. *206*, 29–38.
38. Meireles, D.A., Domingos, R.M., Gaiarsa, J.W., Ragnoni, E.G., Bannitz-Fernandes, R., da Silva Neto, J.F., de Souza, R.F., and Netto, L.E.S. (2017). Functional and evolutionary characterization of Ohr proteins in

eukaryotes reveals many active homologs among pathogenic fungi. Redox Biol. *12*, 600–609.

39. Bolger, A.M., Lohse, M., and Usadel, B. (2014). Trimmomatic: a flexible trimmer for Illumina sequence data. Bioinformatics *30*, 2114–2120.
40. Haas, B.J., Papanicolaou, A., Yassour, M., Grabherr, M., Blood, P.D., Bowden, J., Couger, M.B., Eccles, D., Li, B., Lieber, M., et al. (2013). De novo transcript sequence reconstruction from RNA-seq using the Trinity platform for reference generation and analysis. Nat. Protoc. *8*, 1494–1512.
41. Schmieder, R., and Edwards, R. (2011). Fast identification and removal of sequence contamination from genomic and metagenomic datasets. PLoS ONE *6*, e17288.
42. Huerta-Cepas, J., Forslund, K., Coelho, L.P., Szklarczyk, D., Jensen, L.J., von Mering, C., and Bork, P. (2017). Fast Genome-Wide Functional Annotation through Orthology Assignment by eggNOG-Mapper. Mol. Biol. Evol. *34*, 2115–2122.
43. Altschul, S.F., Gish, W., Miller, W., Myers, E.W., and Lipman, D.J. (1990). Basic local alignment search tool. J. Mol. Biol. *215*, 403–410.
44. Huerta-Cepas, J., Serra, F., and Bork, P. (2016). ETE 3: Reconstruction, Analysis, and Visualization of Phylogenomic Data. Mol. Biol. Evol. *33*, 1635–1638.
45. Jones, P., Binns, D., Chang, H.-Y., Fraser, M., Li, W., McAnulla, C., McWilliam, H., Maslen, J., Mitchell, A., Nuka, G., et al. (2014). InterProScan 5: genome-scale protein function classification. Bioinformatics *30*, 1236–1240.
46. Emanuelsson, O., Nielsen, H., Brunak, S., and von Heijne, G. (2000). Predicting subcellular localization of proteins based on their N-terminal amino acid sequence. J. Mol. Biol. *300*, 1005–1016.
47. Almagro Armenteros, J.J., Salvatore, M., Emanuelsson, O., Winther, O., von Heijne, G., Elofsson, A., and Nielsen, H. (2019). Detecting sequence signals in targeting peptides using deep learning. Life Sci Alliance *2*, e201900429.
48. Fukasawa, Y., Tsuji, J., Fu, S.-C., Tomii, K., Horton, P., and Imai, K. (2015). MitoFates: improved prediction of mitochondrial targeting sequences and their cleavage sites. Mol. Cell. Proteomics *14*, 1113–1126.
49. Almagro Armenteros, J.J., Sønderby, C.K., Sønderby, S.K., Nielsen, H., and Winther, O. (2017). DeepLoc: prediction of protein subcellular localization using deep learning. Bioinformatics *33*, 3387–3395.
50. Kozlowski, L.P. (2016). IPC - Isoelectric Point Calculator. Biol. Direct *11*, 55.
51. Seppey, M., Manni, M., and Zdobnov, E.M. (2019). BUSCO: Assessing Genome Assembly and Annotation Completeness. Methods Mol. Biol. *1962*, 227–245.
52. Katoh, K., Misawa, K., Kuma, K., and Miyata, T. (2002). MAFFT: a novel method for rapid multiple sequence alignment based on fast Fourier transform. Nucleic Acids Res. *30*, 3059–3066.
53. Katoh, K., Kuma, K., Toh, H., and Miyata, T. (2005). MAFFT version 5: improvement in accuracy of multiple sequence alignment. Nucleic Acids Res. *33*, 511–518.
54. Criscuolo, A., and Gribaldo, S. (2010). BMGE (Block Mapping and Gathering with Entropy): a new software for selection of phylogenetic informative regions from multiple sequence alignments. BMC Evol. Biol. *10*, 210.
55. Stamatakis, A. (2014). RAxML version 8: a tool for phylogenetic analysis and post-analysis of large phylogenies. Bioinformatics *30*, 1312–1313.
56. Whelan, S., Irisarri, I., and Burki, F. (2018). PREQUAL: detecting non-homologous characters in sets of unaligned homologous sequences. Bioinformatics *34*, 3929–3930.
57. Ali, R.H., Bogusz, M., and Whelan, S. (2019). Identifying Clusters of High Confidence Homologies in Multiple Sequence Alignments. Mol. Biol. Evol. *36*, 2340–2351.
58. Capella-Gutiérrez, S., Silla-Martínez, J.M., and Gabaldón, T. (2009). trimAl: a tool for automated alignment trimming in large-scale phylogenetic analyses. Bioinformatics *25*, 1972–1973.
59. Nguyen, L.-T., Schmidt, H.A., von Haeseler, A., and Minh, B.Q. (2015). IQ-TREE: a fast and effective stochastic algorithm for estimating maximum-likelihood phylogenies. Mol. Biol. Evol. *32*, 268–274.
60. Lartillot, N., Rodrigue, N., Stubbs, D., and Richer, J. (2013). PhyloBayes MPI: phylogenetic reconstruction with infinite mixtures of profiles in a parallel environment. Syst. Biol. *62*, 611–615.
61. Søndergaard, D., Pedersen, C.N.S., and Greening, C. (2016). HydDB: A web tool for hydrogenase classification and analysis. Sci. Rep. *6*, 34212.
62. Eddy, S.R. (2011). Accelerated Profile HMM Searches. PLoS Comput. Biol. *7*, e1002195.
63. Gawryluk, R.M.R., Kamikawa, R., Stairs, C.W., Silberman, J.D., Brown, M.W., and Roger, A.J. (2016). The Earliest Stages of Mitochondrial Adaptation to Low Oxygen Revealed in a Novel Rhizarian. Curr. Biol. *26*, 2729–2738.
64. Füssy, Z., Vinopalová, M., Treitli, S.C., Pánek, T., Smejkalová, P., Čepička, I., Doležal, P., and Hampl, V. (2021). Retortamonads from vertebrate hosts share features of anaerobic metabolism and pre-adaptations to parasitism with diplomonads. Parasitol. Int. *82*, 102308.
65. Wang, H.-C., Minh, B.Q., Susko, E., and Roger, A.J. (2018). Modeling Site Heterogeneity with Posterior Mean Site Frequency Profiles Accelerates Accurate Phylogenomic Estimation. Syst. Biol. *67*, 216–235.
66. Fu, L., Niu, B., Zhu, Z., Wu, S., and Li, W. (2012). CD-HIT: accelerated for clustering the next-generation sequencing data. Bioinformatics *28*, 3150–3152.
67. Price, M.N., Dehal, P.S., and Arkin, A.P. (2010). FastTree 2–approximately maximum-likelihood trees for large alignments. PLoS ONE *5*, e9490.
68. Minh, B.Q., Schmidt, H.A., Chernomor, O., Schrempf, D., Woodhams, M.D., von Haeseler, A., and Lanfear, R. (2020). IQ-TREE 2: New Models and Efficient Methods for Phylogenetic Inference in the Genomic Era. Mol. Biol. Evol. *37*, 1530–1534.
69. Nývltová, E., Stairs, C.W., Hrdý, I., Rídl, J., Mach, J., Pačes, J., Roger, A.J., and Tachezy, J. (2015). Lateral gene transfer and gene duplication played a key role in the evolution of Mastigamoeba balamuthi hydrogenosomes. Mol. Biol. Evol. *32*, 1039–1055.
70. Leger, M.M., Eme, L., Stairs, C.W., and Roger, A.J. (2018). Demystifying Eukaryote Lateral Gene Transfer (Response to Martin 2017 DOI: 10.1002/bies.201700115). BioEssays *40*, e1700242.
71. Stairs, C.W., Dharamshi, J.E., Tamarit, D., Eme, L., Jørgensen, S.L., Spang, A., and Ettema, T.J.G. (2020). Chlamydial contribution to anaerobic metabolism during eukaryotic evolution. Sci. Adv. *6*, b7258.
72. Stairs, C.W., Kokla, A., Ástvaldsson, Á., Jerlström-Hultqvist, J., Svärd, S., and Ettema, T.J.G. (2019). Oxygen induces the expression of invasion and stress response genes in the anaerobic salmon parasite Spironucleus salmonicida. BMC Biol. *17*, 19.

STAR★METHODS

KEY RESOURCE TABLE

REAGENT or RESOURCE	SOURCE	IDENTIFIER
Chemicals, peptides, and recombinant proteins		
NaCl	Penta	Catalog number: 16610-31000
KCl	Sigma	Catalog number: P5405
$CaCl_2$ dihydrate	Sigma	Catalog number: C7902
$MgCl_2$ hexhydrate	Sigma	Catalog number: M2670
$MgSO_4$ heptahydrate	Carl Roth	Catalog number: P027.2
$NaHCO_3$	Sigma	Catalog number: S5761
Cerophyll	Ward's Science	Catalog number: 470300-680
TRIzol reagent	ThermoFisher Scientific (Invitrogen/Life Technologies)	Catalog number: 15596-026
Dynabeads Oligo(dT)25 kit	ThermoFisher Scientific (Invitrogen/Life Technologies)	Catalog number: 61002
Critical commercial assays		
NEXTflex RNA-Seq Kit	PerkinElmer (BIOO Scientific)	Catalog number: 5129-01
Ribo-Zero Gold Kit	Epicenter, Illumina	Catalog number: MRZE706
Deposited data		
Anaeramoeba ignava (transcriptome)	Genbank: BioProject PRJNA756164 Biosample SAMN20857051	Assembly available at FigShare: https://figshare.com/articles/dataset/Anaeramoebae_are_deeply-branching_eukaryotes_that_clarify_the_transition_from_anaerobic_mitochondria_to_hydrogenosomes/122055177
Anaeramoeba flamelloides (transcriptome)	Genbank: Bioproject PRJNA756164 Biosample SAMN20857050	Assembly available at FigShare:https://figshare.com/articles/dataset/Anaeramoebae_are_deeply-branching_eukaryotes_that_clarify_the_transition_from_anaerobic_mitochondria_to_hydrogenosomes/12205517
Phylogenetic trees and alignments	FigShare: https://doi.org/10.6084/m9.figshare.12205517.v1	FigShare:https://figshare.com/articles/dataset/Anaeramoebae_are_deeply-branching_eukaryotes_that_clarify_the_transition_from_anaerobic_mitochondria_to_hydrogenosomes/12205517
Experimental models: Organisms/strains		
Anaeramoeba flamelloides strain BUSSELTON2	[5]	N/A
Anaeramoeba ignava strain BMAN	[5]	N/A
Software and algorithms		
trimmomatic v0.32	[39]	RRID:SCR_011848; https://github.com/timflutre/trimmomatic
trinityrnaseq_r20140717	[40]	RRID:SCR_013048; https://github.com/trinityrnaseq/trinityrnaseq/
DeconSeq v0.1	[41]	RRID:SCR_007006; http://deconseq.sourceforge.net/)
TransDecoder v5.5	Github: https://transdecoder.github.io/	RRID:SCR_017647;
eggnog-mapper-1.0.3, (database 4.5.1)	[42]	RRID:SCR_021165; https://github.com/eggnogdb/eggnog-mapper
BLAST 2.8.0+	[43]	RRID:SCR_004870; https://blast.ncbi.nlm.nih.gov/Blast.cgi?CMD=Web&PAGE_TYPE=BlastDocs&DOC_TYPE=Download
ETE3	[44]	http://etetoolkit.org/documentation/ete-view/
InterProScan v 5.22-61.0	[45]	RRID:SCR_005829;

(*Continued on next page*)

Continued

REAGENT or RESOURCE	SOURCE	IDENTIFIER
TargetP 1.0	[46]	RRID:SCR_019022; http://www.cbs.dtu.dk/services/TargetP-1.1/index.php
TargetP 2.0	[47]	RRID:SCR_019022; http://www.cbs.dtu.dk/services/TargetP/
MitoFates 1.2	[48]	http://mitf.cbrc.jp/MitoFates/cgi-bin/top.cgi
DeepLoc 1.0	[49]	http://www.cbs.dtu.dk/services/DeepLoc/
Isoelectric Point Calculator v 2.0	[50]	http://isoelectric.org/
BUSCOv 4.0.4 (eukaryota_odb10)	[51]	https://busco.ezlab.org/
mafft v5, v7	[52,53]	RRID:SCR_011811;https://mafft.cbrc.jp/alignment/software/
BMGE v1.12	[54]	https://bioweb.pasteur.fr/packages/pack@BMGE@1.12
RAxML v8	[55]	RRID:SCR_006086; https://cme.h-its.org/exelixis/web/software/raxml/
PREQUAL v1.02	[56]	https://github.com/simonwhelan/prequal
DIVVIER v1.01	[57]	https://github.com/simonwhelan/Divvier
trimAL v1.04	[58]	RRID:SCR_017334; http://trimal.cgenomics.org/
IQ-TREE v1.6, v2.0	[59]	RRID:SCR_017254;
PhyloBayes MPI v1.5	[60]	RRID:SCR_006402; https://github.com/bayesiancook/pbmpi
HydDB v1	[61]	https://services.birc.au.dk/hyddb/
hmmer 3.2.1 (hmmscan)	[62]	RRID:SCR_005305; http://hmmer.org

RESOURCE AVAILABILITY

Lead contact

Further information and requests for resources should be directed to and will be fulfilled by the lead contact, courtney.stairs@biol.lu.se

Materials availability

This study did not generate new unique reagents.

Data and code availability

RNA sequencing reads are deposited on the short-read archive (SRA) with Bioproject number Genbank: PRJNA756164 for *Anaeramoeba ignava* (Biosample Genbank: SAMN20857051) and *Anaeramoeba flamelloides* (Biosample Genbank: SAMN20857050). Assemblies, gene and protein predictions, and phylogenetic datasets have been deposited and are publicly available as of the date of publication at FigShare: https://doi.org/10.6084/m9.figshare.12205517.v1. Any additional information required to reanalyze the data reported in this paper is available from the lead contact upon request.

EXPERIMENTAL MODEL AND SUBJECT DETAILS

Culturing conditions for *Anaeramoeba ignava* and *Anaeramoeba flamelloides*

Strain BUSSELTON2 of *Anaeramoeba flamelloides* and strain BMAN of *Anaeramoeba ignava* were maintained in monoeukaryotic culture with unidentified prokaryotes in ATCC medium 1525 at room temperature and were sub-cultured once a week.[5] ATCC medium 1525 was prepared with artificial seawater (Final concentration: 24.71 g/L NaCl; 0.68 g/L KCl; 1.36 g/L $CaCl_2$ dihydrate; 4.66 g/L MgCl2 hexahydrate; 6.3 g/L $MgSO_4$ heptahydrate; 0.18 g/L $NaHCO_3$; 0.5 g/L Na_2HPO4; 2.5 g/L Cereal Grass Media).

METHOD DETAILS

RNA isolation and sequencing

RNA was isolated from 80 (*A. flamelloides*) or 360 (*A. ignava*) ml of high-density culture, using TRIzol Reagent (ThermoFisher Scientific) following the manufacturer's protocol. Briefly, *A. flamelloides* cells were grown in 25-cm^2 culture flasks sealed with 40 mL of culture medium. For RNA extraction, liquid medium was removed by decanting from each flask and 5 mL of TRIzol the culture ('adherent cells' protocol). *A. ignava* cells were grown in 36 10 mL plastic tubes. Cells were collected by centrifugation (800 x g

for 10 min) at room temperature. For RNA extraction, a total of 15 mL of TRIzol was used to resuspend and combine the pellets from the 36 tubes ('suspension cells' protocol). Messenger RNA was purified by multiple steps (3 steps of mRNA selection for BMAN, 2 steps for BUSSELTON2) using Dynabeads Oligo(dT)25 kit (Life Technologies) and in the case of BUSSELTON2 ribodepletion was performed by Ribo-Zero Gold Kit (Epicenter, Illumina). Illumina compatible RNaseq libraries were prepared using the NEXTflex RNA-Seq Kit (BIOO Scientific). 150 bp paired end reads were sequenced on the MiSeq platform and quality-filtered by the Genomics and Bioinformatics Core Facility, IMG Academy of Sciences of the Czech Republic (BUSSELTON2) and the Genomics Core Facility, EMBL, Heidelberg (BMAN).

Read decontamination, transcriptome assembly, and annotation

Read statistics before and after decontamination are shown in Data S1. Adaptor trimming was performed using trimmomatic v0.32 using recommended settings (SLIDINGWINDOW:10:25 MINLEN:50).[39] Initial assemblies were performed using Trinity (trinityrnaseq_r20140717[40]) using default parameters. The top 100 most abundant transcripts were extracted and used as queries against the *nt* database on GenBank to identify potential contaminants using a cut-off of 90% sequence identity. Genomes of those organisms most similar to the trinity transcripts were downloaded (Data S1) and used to decontaminate the raw reads using DeconSeq[41] (http://deconseq.sourceforge.net/). 'Cleaned' reads were reassembled using Trinity with default parameters. TransDecoder v5.5 was used to predict the open-reading frames and protein sequences for all transcripts (https://github.com/TransDecoder/TransDecoder/). Transcriptome completeness was assessed using BUSCO[51] v 4.0.4 (eukaryota_odb10 (eukaryota, 2019-11-20)). We recovered 61% and 47% of near-universal single-copy orthologs for each species, respectively, which is comparable to the BUSCO coverage for complete genomes and deeply sequenced transcriptomes of other metamonads (Data S1). Putative protein sequences were annotated using eggNOG-mapper (emapper-1.0.3, emapper DB: 4.5.1).[42] Each protein sequence was queried against the *nr* database using BLAST 2.8.0+[43] and the taxonomic provenance of the top hit was assigned with ete3.[44] The completeness measures assigned by TransDecoder for each open reading frame was manually investigated to determine whether the sequence was full-length, 5′-partial, 3′-partial or internal (5′- and 3′-partial) using BLAST again the nr database, see Data S1. We manually corrected some protein models predicted by TransDecoder that extended into the 5′ untranslated region of the transcripts based on homology to other sequences in GenBank. Interpro (IPR) domains were annotated using interproscan[45] with the iprdomain setting. Subcellular localization was predicted using TargetP,[46] TargetP2,[47] MitoFates,[48] and DeepLoc[49] and summarized in Data S1. Net charge of putative N-terminal targeting signals was calculated at pH 5.5, 7.4 and 8.0 using Isoelectric Point Calculator[50] (v. 2.0). For each prediction software, we arbitrarily assigned a confidence point of one for any prediction with the probability of mitochondrial localization greater than 0.5 and a point of 0.5 if the probability of mitochondrial localization was less than 0.5 but the software still predicted mitochondrial localization. Every protein with one confidence point was manually investigated for mitochondrial provenance. Putative MRO proteins from other free-living anaerobic protists (*Pygsuia biforma*,[21] *Brevimastigomonas motovehiculus*[63]) were used as queries against the protein datasets of each transcriptome to identify similar homologs (-evalue 0.001).

Phylogenomic dataset assembly

To infer the phylogenetic placement of the two *Anaeramoeba* species, we updated a previously published phylogenomic dataset of 155 proteins[3] by adding orthologs from the Anaeramoebae, and three recently published metamonads, *Retortamonas dobelli*,[64] *Retortamonas* cf. *caviae*,[64] and *Barthelona* sp.[7] For each of the 155 proteins, we used the *Arabidopsis thaliana* or *Homo sapiens* homolog as a query against the predicted proteins of each *Anaeramoeba* species (e-value cut-off = 10e-10) using BLASTP[43] and retained up to five hits. Those potential homologs were then used as queries for a reciprocal BLAST search against a dataset containing the initial set of identified orthologs, but also their known deep paralogs (i.e., corresponding to duplications predating the last eukaryotic common ancestor, such as EF1-L and EF1-α). *Anaeramoeba* sequences were retained for subsequent analyses if their reciprocal best BLAST hit belonged to the orthologous clade of interest. These were added to the existing ortholog dataset, which was aligned using mafft-linsi.[52,53] Ambiguously aligned positions were trimmed using BMGE v1.12 (default settings, except from -m BLOSUM62 and -g 0.3;[54]). Preliminary maximum likelihood individual protein trees were computed using RAxML v8 (with the PROTGAMMALG model, branch support was estimated using 100 rapid bootstraps).[55] For the three recently published metamonads, all previously identified orthologs were used as queries against the predicted proteins for each species (e-value cut-off = 10e-5) using BLASTP[43] and retained up to five hits per query. These were added to the existing dataset, filtered for sequencing errors and non-homologous sites using PREQUAL,[56] aligned using mafft-ginsi,[52,53] alignment uncertainty and errors were filtered using DIVVIER,[57] and the filtered alignments were trimmed of sites comprised of > 99% gaps using trimAL (-gt 0.01).[58] Preliminary maximum likelihood individual protein trees were estimated using IQ-TREE under the LG+C20+F+G model, and branch support was estimated using 100 RAxML rapid bootstraps inferred using the LG4X model. Each tree was then manually inspected and a single sequence corresponding to the correct ortholog was selected for each species. In case of in-paralogs specific to the newly added taxa, the sequence with the best coverage of the alignment or the shortest branching sequence was selected. Single protein trees were recomputed as previously described, and well-supported bipartitions (bootstrap support > 70) were further investigated to identify potential paralogs, contaminants, or lateral- or endosymbiotic gene transfers, which were then removed from the datasets. Final datasets were realigned and trimmed as described for the recently published Metamonada species and concatenated into a single large alignment (supermatrix containing 95 sequences and 53637 sites). Unaligned individual protein sequences have been deposited in a Figshare https://doi.org/10.6084/m9.figshare.12205517.v1.

Phylogenomic tree reconstruction

Maximum likelihood (ML) phylogenies were inferred using IQ-TREE v1.6[59] under the LG+C60+F+G mixture model. Statistical confidence was derived from 1000 non-parametric bootstraps using the site-heterogeneous LG+C60+F+G+PMSF with posterior mean site frequencies (PMSF) using the LG+C60+F+G ML tree as guide tree.[65] The supermatrix was also subjected to a Bayesian analysis with PhyloBayes MPI v1.5[60] under the CAT + GTR + G model (default settings). Four independent Markov chain Monte Carlo chains were run for ~6000 generations. Three of the four chains favored different topologies where Metamonada was not monophyletic. Instead two separate clades comprised of parabasalids+*Anaeramoeba* and *Barthelona*+Fornicata+Preaxostyla branched sequentially in the eukaryote tree. The fourth chain recovered Metamonada as monophyletic with Parabasalia+*Anaeramoeba* branching sister to *Barthelona*+ fornicates+preaxostylids. In all chains, *Anaeramoeba* species grouped with parabasalids.

QUANTIFICATION AND STATISTICAL ANALYSIS

Investigation of select relationships in the phylogenomic analyses

Since the addition of *Anaeramoeba* fundamentally altered the relationships of Metamonada in the ML tree, by recovering Preaxostyla+Fornicata rather than Parabasalia+Fornicata, we conducted AU tests to investigate support for this, and other relationships between excavates. We inferred ML trees using IQ-TREE under the LG+C60+F+G model, constraining the monophyly of Parabasalia+Fornicata+*Barthelona*, Parabasalia+Fornicata+*Barthelona*+*Anaeramoeba,* C*ollodictyon*+*Malawimonas*+Discoba+Metamonada, and Discoba+Metamonada, as well as the Bayesian consensus topology (that recovered paraphyletic metamonads) using the -g option. The AU test was implemented in IQ-TREE on our ML topology, the individual constrained trees, and 100 distinct local topologies saved during ML analysis of our concatenated dataset (-wt option in IQ-TREE). Newick formatted constraint topologies are provided (https://doi.org/10.6084/m9.figshare.12205517.v1). Topologies that returned an AU-test p-value less than 0.05 were considered rejected. See Data S1 for a complete summary.

Investigation of select relationships in phylogenetic analyses of genes related to hydrogen metaoblism and the oxygen stress response

The initial dataset of *Anaeramoeba* hydrogenase proteins was built by retrieving any sequence containing the large hydrogenase domain (IPR004108) based on the InterProScan annotations. These proteins were subclassified as Group A or Group B using HydDB[61] and separated for the following analyses. For the Group A and Group B sequences, we first extracted the hydrogenase domain using hmmscan[62] (http://hmmer.org) and the Pfam hmm profile PF02906.12 (Fe_hyd_lg_C) or TIGR04105 from TIGR, using default settings, respectively. These sequences were used as queries against the non-redundant database (*nr*) and a local database of metamonad sequences[3] using BLAST[43] (e-value < 1e-10; -max_target_seqs 1500). Sequences from these BLAST results were combined and reduced using cd-hit[66] (-c 0.8). The retrieved Group A and Group B sequences were subclassified as above with HydDB[61] and only the regions corresponding to the large hydrogenase domain was extracted as above. For initial datasets, sequences were aligned using mafft-linsi[52] and trimmed using BMGE[54] (v1.12; -h 0.7, -m BLOSUM30) and the phylogeny was generated using FastTree2.[67] Trees were manually inspected to identify those clades that were distantly related to the sequences of interest that could be removed to reduce the size of the dataset. Final datasets were aligned using mafft-linsi and trimmed with BMGE as above. Phylogenies were inferred using IQTREE[68] v2.0 under the best scoring model of evolution decided by ModelFinder (supplemented with the C-series mixture models with -mset LG+C20,LG+C10,LG+C60,LG+C30,LG+C40,LG+C50) and 1000 ultrafast bootstraps (-bb 1000). The resulting maximum likelihood tree was used as a guide tree to compute 100 non-parametric bootstraps using the PMSF framework[65] implemented in IQTREE.[68] Model parameters and alignment features can be found in Data S1. Constrained estimation of topologies conditional on enforcing the monophyly of eukaryotes were performed in IQTREE as described above (Data S1).

Phylogenetic analyses demonstrated that the *Anaeramoeba* Group A sequences branched in a large clade composed of eukaryotic and prokaryotic sequences (i.e., *Thermotogales*) similar to previous analyses[69–71] (Figure S2). We conducted approximately unbiased (AU) tests to determine if alternative topologies could be rejected by these data. We inferred ML trees using IQ-TREE under the best-scoring model of evolution for each gene as decided by ModelFinder (supplemented with the C-series mixture models with -mset LG+C20,LG+C10,LG+C60,LG+C30,LG+C40,LG+C50) constraining the topologies listed in Data S1 using the -g option. The AU test was implemented in IQ-TREE on our ML topology, the individual constrained trees, and 100 distinct local topologies saved during ML analysis of our concatenated dataset (-wt option in IQ-TREE). Topologies that returned an AU-test p-value less than 0.05 were considered rejected. See Data S1 for a complete summary.

Topologies constraining the monophyly of eukaryotes, or Parabasalia+*Anaeramoeba* were not rejected (Data S1). However, the AU-test rejected the topology constraining the monophyly of Metamonada (p = 0.00874, Data S1) suggesting that the metamonad hydrogenases might not share a most recent common ancestor or that other eukaryotic taxa received a metamonad-like hydrogenase after the split of *Anaeramoeba*+Parabasalia and Preaxostyla+*Barthelona*+Fornicata. Group B sequences were only found in Preaxostyla, Amoebozoa, and the anaeramoebids indicating they are less widespread among eukaryotes compared to the Group A paralog. In phylogenetic analyses, the *Anaeramoeba* Group B sequences formed a clade with *Entamoeba* and *Mastigamoeba* sequences; however, this relationship was poorly supported (BP = 13; Figure S3).

For FDP and OsmC analyses we added the *Anaeramoeba* sequences to datasets presented in Stairs et al. (2019)[72] and Meireles et al. (2017),[38] respectively. Datasets were aligned with mafft and trimmed with BMGE, as above. Phylogenies were inferred using

IQTREE[68] v2.0 under the best scoring model of evolution decided by ModelFinder (supplemented with the C-series mixture models with -mset LG+C20,LG+C10,LG+C60,LG+C30,LG+C40,LG+C50) and 1000 ultrafast bootstraps (-bb 1000). The resulting maximum likelihood tree was used as a guide tree to compute 100 non-parametric bootstraps using the PMSF framework[65] implemented in IQTREE.[68] Model parameters and alignment features can be found in Data S1. Constrained estimation of topologies conditional on enforcing the monophyly of eukaryotes were performed in IQTREE as described above (Data S1).